Analyst

PAPER

View Article Online
View Journal | View Issue

Cite this: *Analyst*, 2014, **139**, 2832

Differential pulse adsorptive stripping voltammetric determination of nanomolar levels of atorvastatin calcium in pharmaceutical and biological samples using a vertically aligned carbon nanotube/graphene oxide electrode†

Tiago Almeida Silva,[a] Hudson Zanin,[b] Fernando Campanhã Vicentini,[a] Evaldo José Corat[b] and Orlando Fatibello-Filho*[a]

Received 16th January 2014
Accepted 28th February 2014

DOI: 10.1039/c4an00111g

www.rsc.org/analyst

A novel vertically aligned carbon nanotube/graphene oxide (VACNT-GO) electrode is proposed, and its ability to determine atorvastatin calcium (ATOR) in pharmaceutical and biological samples by differential pulse adsorptive stripping voltammetry (DPAdSV) is evaluated. VACNT films were prepared on a Ti substrate by a microwave plasma chemical vapour deposition method and then treated with oxygen plasma to produce the VACNT-GO electrode. The oxygen plasma treatment exfoliates the carbon nanotube tips exposing graphene foils and inserting oxygen functional groups, these effects improved the VACNT wettability (super-hydrophobic) which is crucial for its electrochemical application. The electrochemical behaviour of ATOR on the VACNT-GO electrode was studied by cyclic voltammetry, which showed that it underwent an irreversible oxidation process at a potential of +1.08 V in pH_{cond} 2.0 (0.2 mol L^{-1} buffer phosphate solution). By applying DPAdSV under optimized experimental conditions the analytical curve was found to be linear in the ATOR concentration range of 90 to 3.81 × 10^3 nmol L^{-1} with a limit of detection of 9.4 nmol L^{-1}. The proposed DPAdSV method was successfully applied in the determination of ATOR in pharmaceutical and biological samples, and the results were in close agreement with those obtained by a comparative spectrophotometric method at a confidence level of 95%.

1. Introduction

Carbon nanotubes (CNT) have aroused enormous interest in various sectors of technological development, being one of the most widely studied materials applied in the field of nanotechnology.[1] The large investment recorded in the development of technologies based on CNT is due to their unique optical, electronic and mechanical properties. Carbon nanotubes (CNT) have been employed in the preparation of electrochemical sensors and biosensors, enabling the detection of low concentrations of compounds in aqueous solutions.[2–5]

The electrochemical performance of CNT electrodes depends directly on their surface area, conductivity, presence of defects, purity, orientation and chemical functionalisation of the nanostructures.[6–8] A significant part of the literature presumes that the CNT sidewall is inert and that edge-plane-graphite-like open ends and defect sites are responsible for the electron transfer activity observed.[9] These studies have generally been performed using multiwalled carbon nanotube (MWCNT) electrodes and claim that these electrodes exhibit similar behaviour to single-walled carbon nanotube (SWCNT) electrodes.[10] In contrast, studies of well characterised SWCNT electrodes, either as individual tubes or as two-dimensional networks, suggest sidewall activity.[10] It is evident that the majority of reports infer the contribution of "defects" in the electrochemistry of CNT electrodes largely from cyclic voltammetric analysis. While defects may play an important role in the electrochemistry of certain species, especially those that react *via* surface-mediated "inner-sphere" electron transfer, there is still no direct high resolution electrochemical evidence that a nanotube sidewall is completely inactive.[11] However, electrodes having vertically aligned carbon nanotubes (VACNT) have been demonstrated to display better electrochemical responses than those with randomly oriented nanotubes,[6,7,12,13] which can be explained by the high density of edge-plane-graphite sites which are exposed in this CNT orientation.[7] Additionally, the

[a]*Department of Chemistry, Federal University of São Carlos, Rod. Washington Luís km 235, P. O. Box 676, São Carlos, CEP: 13560-970, SP, Brazil. E-mail: bello@ufscar.br; Fax: +55 16 33518350; Tel: +55 16 33518098*

[b]*National Institute for Space Research, Av. dos Astronautas 1758, São José dos Campos, CEP: 12227-010, SP, Brazil*

† Electronic supplementary information (ESI) available. See DOI: 10.1039/c4an00111g

electrochemical behaviour of CNT electrodes significantly improves after oxygen functional groups are inserted along the length of their surface.[9,14,15] These oxygenated sites are believed to improve the local electron transfer rate.[16] A few studies have produced as grown CNT with longitudinal exfoliated graphene structures.[17–19] If VACNT have a better electrochemical response due to the high density of sp^2 edge planes at their tips and if oxygen functional groups may improve the local electron transfer rate it is quite probable that the electrochemical performance will be enhanced by enhancing such characteristics. The exfoliation of VACNT tips would significantly increase the edge plane density by exposing the structure of the graphene inner. Oxidation is the main exfoliation method, which results in graphene oxide (GO) with plenty of functional groups. We have recently published details of such an electrode material which was developed by oxygen plasma exfoliation of VACNT tips.[18] The electrode material was shown to have excellent electrochemical properties with a very highest transfer rate (3.4×10^{-2} cm s^{-1}).

Recently, a number of studies have been devoted to the development of sensors using electrodes containing oriented nanotubes. These include electrochemical sensors which have been developed using VACNT electrodes to determine the identity and concentration of pharmaceuticals in commercial products and biological samples. Examples of analytes of interest are: bisphenol A,[13] uric acid,[20] glucose,[21] hydrogen peroxide[22] and dopamine.[23]

Atorvastatin calcium (ATOR) is a synthetic drug from the statin family which is used for the treatment of dyslipidemia and the prevention of cardiovascular diseases.[24] ATOR acts to reduce the level of cholesterol in blood plasma by inhibiting the activity of the enzyme 3-hydroxy-3-methylglutaryl CoA reductase (HMG-CoA reductase), which catalyzes the production of mevalonic acid, the precursor in the cholesterol biosynthesis.[25] In humans, ATOR is rapidly absorbed after oral administration, reaching the maximum peak absorption in the blood plasma ($\approx$98.0%) in 0.5–1.5 h.[24,26] Its half-life in human blood plasma is between 15 and 30 h, due to the action of other active metabolites. Fecal excretion is the main route for ATOR elimination, with a lower contribution by renal excretion (<2.0%).[24,26] Due to the pharmacological importance of ATOR, the control of its concentration in commercial formulations is essential to guarantee its success in the treatment of patients with this drug, and, for pharmacokinetic studies, highly sensitive analytical methods are necessary due to the low level of this compound usually found in biological samples.

The analysis and quantification of ATOR has been reported by high-performance liquid chromatography,[27] capillary electrophoresis,[28,29] spectrofluorimetry,[30] spectrophotometry[31] and FT-Raman spectroscopy.[32] In these methods, expensive equipment is needed, the analysis time is relatively high (especially due to the pre-steps of sample preparation) and skilled labour is required. Thus, there is an increasing requirement to investigate alternative analytical methods for ATOR determination which are simple, inexpensive and fast. Electroanalytical methods offer some interesting advantages compared to traditional methods, such as relative operational simplicity, low cost, and also the possibility of the direct determination of analytes without (or with minimal) sample preparation steps by voltammetric techniques.[33,34] Among the existing voltammetric techniques, differential pulse adsorptive stripping voltammetry (DPAdSV) is interesting because it involves the pre-concentration of the analyte molecules on the surface of the working electrode, which can improve the analytical sensitivity and limit of detection. Thus, some studies have been published where electroanalytical methodologies are proposed for ATOR detection.[35–37] Nevertheless, there are few reports on the electroanalytical determination of ATOR in pharmaceutical and biological samples, and none which use VACNT electrodes.

In this paper, we describe the development of a new DPAdSV method for the determination of ATOR in pharmaceutical and biological samples using the new oxygen plasma exfoliated VACNT, or VACNT-GO, electrode. This work reports for the first time the high sensitivity of VACNT-GO as an electrochemical sensor for a pharmaceutical analyte. It proves to be very promising in electroanalysis.

2. Experimental

2.1. Reagents and solutions

ATOR and methanol of HPLC grade were purchased from Sigma-Aldrich. The stock solutions of ATOR were prepared in methanol, due to its better solubility in this solvent. All other chemical reagents used were of analytical grade, and the solutions were prepared in ultra-pure water with a resistivity greater than 18.0 MΩ cm supplied by a Millipore Milli-Q system (Billerica, USA).

2.2. Synthesis and characterisation of vertically aligned carbon nanotube/graphene oxide nanocomposite

VACNT films were prepared by microwave chemical vapour deposition (MWCVD) using a microwave-plasma chamber at 2.45 GHz.[18,38] The substrate used was a Ti sheet (10 mm × 10 mm × 0.5 mm) covered with a 10 nm Ni layer deposited by electron-beam evaporation. This Ti substrate/Ni layer was heated in a N_2/H_2 (10/90 sccm) plasma from 350 to 800 °C over a period of 5 min, which caused it to ball up into nanoclusters that subsequently became the catalyst particles for VACNT growth. Next, CH_4 (14 sccm) was introduced into the chamber for 1 min, maintaining a substrate temperature of 800 °C. The reactor pressure was 30 Torr during all the procedures. The VACNT films were then given an oxygen plasma treatment in order to partially exfoliate the ends of the carbon nanotubes and to incorporate oxygen-containing groups (–OH, –COOH, =O). This exfoliation and functionalisation was performed using a pulsed-DC (−700 V, pulse frequency 20 kHz) plasma reactor with an oxygen flow rate of 1 sccm at a pressure of 150 mTorr.[39] After this functionalisation we renamed the samples as vertically aligned carbon nanotube/graphene oxide nanocomposites (VACNT-GO).

All the samples were characterized by scanning electron microscopy (SEM), Raman spectroscopy, X-ray photoelectron spectroscopy (XPS) and surface wettability. All the

measurements were conducted at room temperature. The SEM measurements were performed using a field emission scanning electron microscope (JEOL6330) to evaluate the structural arrangements and to monitor the modification of the surface morphology. Laser Raman spectroscopy (Renishaw 2000 system, Ar^+-ion laser excitation, $\lambda = 514.5$ nm) was used in backscattering geometry to analyse the structural changes of the samples. The curve fitting and data analysis software Fityk assigned the peak locations and corresponding fitting of all the spectra. X-ray photoelectron spectroscopy (VSW – HA100, using Al(Kα) radiation, 1486.6 eV) was used to identify the oxygen content and bonding type on the sample surface. Surface area measurements were carried out using the Quantachrome NovaWin model 1000 for multi-point BET using the classical helium-void volume method.[38] A Krüss Easy Drop system in the sessile drop mode was used to measure the contact angle (CA) using high-purity deionised water at room temperature, providing information about the wettability of the VACNT and VACNT-GO films.

2.3. Electrochemical assays and working electrode construction

The electrochemical measurements were performed using an Autolab PGSTAT-30 (EcoChemie, Netherlands) potentiostat/galvanostat driven by GPES 4.9 software. All of the electrochemical experiments were carried out using a Pyrex three-electrode cell comprising an Ag/AgCl (3.0 mol L^{-1} in KCl) reference electrode and a Pt foil as a counter electrode. The Ti substrate containing the VACNT-GO film was immobilised on a copper plate using conductive silver paste, and was used as the working electrode.[18]

2.4. Analytical procedure

We used only one VACNT-GO electrode in the whole development of the voltammetric procedure for ATOR determination. First, we identified the best supporting electrolyte (composition and pH) for the voltammetric response of ATOR. Next, the DPAdSV technique was used to develop the voltammetric method, and therefore all of the relevant experimental parameters for this technique were systematically optimized. Then, using these optimal experimental conditions, analytical curves were constructed using the DPAdS voltammograms recorded after the successive addition of aliquots of the ATOR stock solution into the electrochemical cell containing 10 mL of 0.2 mol L^{-1} phosphate buffer solution (pH_{cond} 2.0, 20% v/v methanol). This allowed the analytical parameters for this voltammetric procedure, such as the linear range of the concentrations and the limit of detection to be determined. The stability of the method was verified from studies of intra-day ($n = 10$) and inter-day ($n = 3$) repeatability. Measurements with several sample VACNT-GO electrodes were performed in order to study their electrochemical response and repeatability.

Three commercial pharmaceutical samples of ATOR were purchased in a local pharmacy (I 10 mg per tablet; II & III 20 mg per tablet). To prepare these samples, ten tablets of each sample were weighed and pulverised to a powder in a mortar and pestle. A suitable amount of each sample (104.73 mg – I; 204.31 mg – II; 309.24 mg – III) was weighed and transferred to a 10 mL volumetric flask and the remaining volume was completed with methanol in order to obtain the ATOR stock solutions for each sample. The samples were subjected to sonication for 10 min. The non-dissolved solids were filtered off. Aliquots of each of the stock solutions were directly transferred to the electrochemical cell and the respective voltammograms were recorded. The ATOR concentration in each sample was determined independently three times using the optimal analytical conditions and procedure described above. The commercial samples were also analysed by UV-Vis spectroscopy ($\lambda = 244$ nm)[40] as a comparison using a Shimadzu UV-2550 spectrophotometer.

The effect of some excipients typically found in pharmaceutical formulations on the DPAdSV measurements was studied. In addition, the effect of the sample matrix was also investigated by addition/recovery experiments performed in triplicate.

In order to test whether ATOR could be determined in solutions containing many different interfering species normally found in biological samples, synthetic substitutes for urine and human serum containing the majority of interferents present in real samples were prepared as previously reported.[41,42] For the synthetic urine sample, 0.73 g of NaCl, 0.40 g of KCl, 0.28 g of $CaCl_2 \cdot 2H_2O$, 0.56 g of Na_2SO_4, 0.35 g of KH_2PO_4, 0.25 g of NH_4Cl and 6.25 g of urea were dissolved in water in a 250 mL volumetric flask.[41] For the preparation of the synthetic human serum sample, 3.0 g of NaCl, 0.16 g of $NaHCO_3$, 3.5 mg of tryptophan, 2.3 mg of glycine, 3.2 mg of serine, 3.7 mg of tyrosine, 6.6 mg of phenylalanine, 9.1 mg of lysine, 6.3 mg of histidine, 29 mg of aspartic acid, 9.1 mg of alanine and 10 mg of arginine were dissolved in water in a 250 mL volumetric flask.[42] ATOR at two different concentrations was then added to the two synthetic biological samples and the samples were analysed directly.

3. Results and discussion

3.1. Material characterisation

Fig. 1(a–f) show typical SEM images of the (a) as-grown VACNT forest and (b–f) exfoliated VACNT structures. Fig. 1(a) shows the as-grown VACNT forest, and highlights its alignment, its high spatial density, and relatively flat, carpet-like surface. The CNT are ~40 μm long and about 40 nm thick; with each CNT nearly touching its neighbour (separation distance is estimated at ~10 nm). Fig. 1(b) is a top view of these carbon nanotubes after oxygen plasma etching, showing the effect of exfoliation. We observed that the oxygen plasma exfoliated the carbon nanotube tips, opening their walls and exposing their fundamental structure: graphene.[18] The tips are known to be the most defective part of nanotubes, which makes this area more sensitive to plasma etching. We observed that the tips etched first, however the oxygen plasma could etch the whole nanotubes if the plasma treatment was performed at a much higher pressure than we used (range from 50 to 300 mTorr) or for a longer time. In addition, from the SEM images one can observe that the VACNT-GO electrode has a highly porous structure. BET

adsorption isotherms showed that the VACNT-GO material had an effective surface area of ~930 m^2 g^{-1}.

The oxygen plasma treatment causes structural modification of the VACNT sample as can be seen in Raman spectra. Fig. S1 (ESI†) shows the first- and second-order Raman spectra of VACNT films before and after plasma treatment. The deconvolutions were performed using Lorentzian line shapes for the D and G bands, and a Gaussian line shape for the bands around 1250 (#), 1480–1520 (*) and 1622 cm^{-1} (D′ shoulder).[43,44] The D band is usually attributed to the disorder and imperfection of the carbon crystallites. The G band is assigned to one of the two E_{2g} modes corresponding to stretching vibrations in the basal plane (sp^2 domains) of single crystal graphite or graphene.[45] The high intensity of the G′ band reveals that these materials have high structural quality. In the Raman first-order spectrum, we found that two Gaussian peaks centred at ~1250 and ~1480 cm^{-1} were required in order to fit the overall spectrum accurately. Probably the 1250 cm^{-1} band has its origin in a double resonance process, because its Raman shift (~1200 cm^{-1}) is a point on the phonon dispersion curves. These results are reproducible and they are in agreement with our previous results.[18,38]

Fig. S2(ESI†) shows (a) C 1s and (b) O 1s fitted XPS spectra recorded from a VACNT sample after plasma treatment. The C 1s curve has been deconvoluted into four peaks at ~284.5, 285.8, 288.5, and 291.6 eV. The peaks correspond to aliphatic carbons (with C–C single bonds), carbon atoms with C–O, C–O–C, or C–OH single bonds, carbon atoms with C═O double bonds, and carbon atoms with the COO– carboxylate bonds, respectively.[18,39] The peak at 291.6 eV is used to assign the shake-up peak (p–p* transitions). The O 1s curve has been deconvoluted into three peaks at around 535.5, 533.5, and 532.3 eV, which correspond to C–O, –COOH, and C–OH, respectively. This implies the formation of strong C–O bonds from the oxygen-containing groups that are situated along the tubes.[46] This suggests that the plasma etching creates open-ended termini in the CNT structures, which are stabilized by –COOH and –OH groups, and which remain bonded to the nanotubes at the end termini and/or sidewall defect sites.

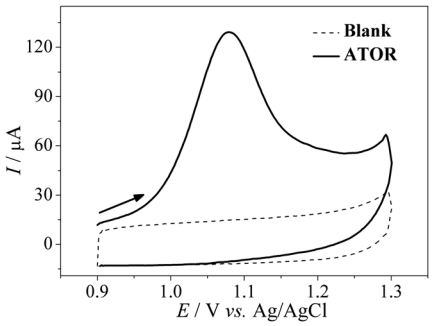

Fig. 2 Cyclic voltammogram obtained for a 5.0×10^{-5} mol L^{-1} ATOR solution in 0.2 mol L^{-1} buffer phosphate (pH_{cond} 2.0) containing 20% (v/v) of methanol, using the VACNT-GO electrode and a potential scan rate, $v = 50$ mV s^{-1}. 'Blank' refers to the control scan taken in the buffer/methanol solution with no ATOR present.

SEM analysis clearly shows that the oxygen plasma acts mainly on the top surface of exfoliated VACNT tips. XPS analysis shows that the plasma treatment increases the oxygen atom content of the samples from 4% up to 18%. The C–O ratio in the measured content is larger than 6, which is outside the range reported for GO (from 1.3 to 2.25).[47] However, the oxygen content is probably concentrated on the top surface while XPS probes an overall sample content. From the SEM images we can say that the length of the carbon nanotubes is around 40 μm and that oxygen etching seems to happen up to only around 10 μm below the VACNT surface. From this a better approach would be to estimate the C–O ratio by dividing by around 4, which is inside the GO reported range.

The surface wettability of the as-grown VACNT and oxidized VACNT-GO samples was compared by measuring the CA between the water drops and the sample surface. The as-grown samples exhibited superhydrophobic behaviour (CA ~ 157°) and the plasma etching changed the behaviour to

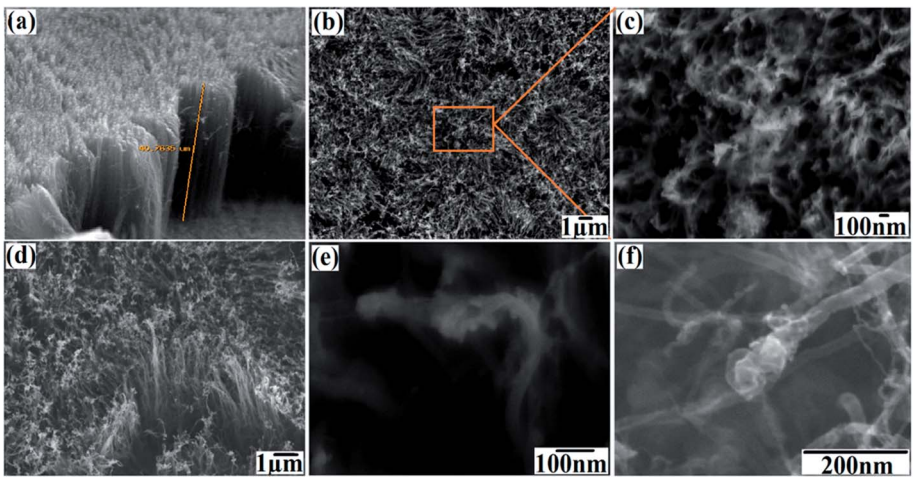

Fig. 1 SEM images of VACNT forest films: (a) as-grown samples; and (b–f) effect of oxygen plasma etching. (b & d) are top view images. (c) Higher magnification of the box in (b). (e & f) Higher magnification of the exfoliated tips.

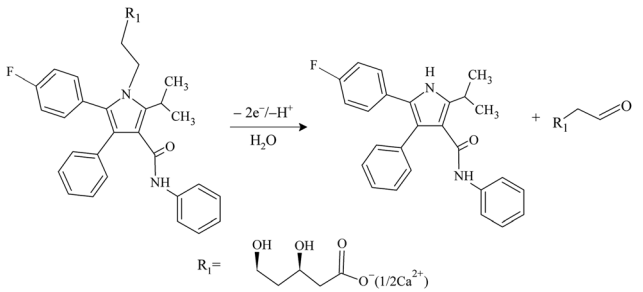

Fig. 3 Suggested electro-oxidation reaction of ATOR (adapted from ref. 37).

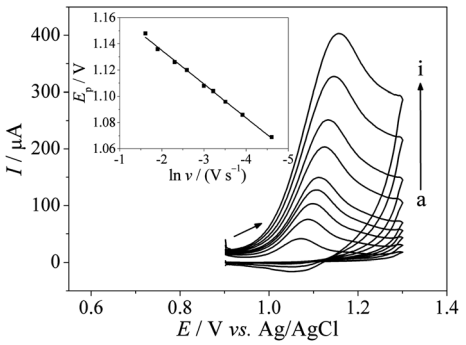

Fig. 4 Cyclic voltammograms obtained for a 5.0×10^{-5} mol L^{-1} ATOR solution in 0.2 mol L^{-1} phosphate buffer (pH_{cond} 2.0, 20% v/v methanol) using the VACNT-GO electrode at different potential scan rates, *v*: (a) 10, (b) 20, (c) 30, (d) 40, (e) 50, (f) 75, (g) 100, (h) 150 and (i) 200 mV s^{-1}. The pre-concentration time was fixed at 180 s. Inset: E_p *vs.* ln *v*.

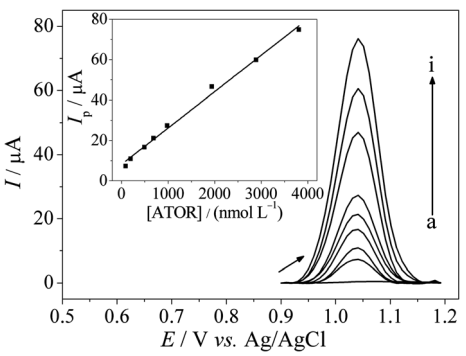

Fig. 5 DPAdS voltammograms obtained for different ATOR concentrations in 0.2 mol L^{-1} phosphate buffer (pH_{cond} 2.0, 20% v/v methanol) using the VACNT-GO electrode: (a) 0.00, (b) 90.0, (c) 200.0, (d) 500.0, (e) 690.0, (f) 980.0, (g) 1940.0, (h) 2890.0 and (i) 3810.0 nmol L^{-1}. The pre-concentration time was fixed at 180 s. Inset: analytical curve.

superhydrophilic (CA $\sim 0°$).[48] To confirm our GO observation at the VACNT tips, some samples were reduced in a short time in a hydrogen plasma to form RGO exfoliated tips. SEM images show a similar exfoliated appearance (not shown) but other characteristics typical of the VACNT-GO samples were lost: Raman spectra similar to the VACNT sample, the superhydrophilic character was lost and, mainly, the electrochemical response was significantly reduced. Because of this the superhydrophobic character of our as-grown samples makes them unsuitable for use as electrodes and we performed the electrochemical measurements just with the VACNT-GO.

3.2. Electrochemical behaviour of ATOR

The electrochemical behaviour of ATOR was investigated by cyclic voltammetry using the VACNT-GO electrode. Fig. 2 shows the cyclic voltammogram obtained for a 5.0×10^{-5} mol L^{-1} ATOR solution in 0.2 mol L^{-1} phosphate buffer solution (pH_{cond} 2.0) containing 20% (v/v) of methanol. The use of this percentage of methanol in the supporting electrolyte was necessary to maintain the drug in solution; the 20% value was previously determined by solubility tests in water/methanol mixtures with different concentrations of alcohol. As can be seen, the voltammogram for the ATOR solution exhibited an oxidation peak at +1.08 V, and no reduction peak was observed. This indicates that ATOR oxidation is an irreversible process, which is in agreement with the literature using different electrodes,[35–37] a glassy carbon electrode (GCE) at +1.03 V,[35] a boron-doped diamond electrode (BDD) at +0.98 V[35] and a carbon paste electrode (CPE) +1.07 V.[37] In addition, Fig. S3 (ESI†) shows the cyclic voltammograms obtained for ATOR solutions using the VACNT-GO electrode and a GCE. As can be seen, the VACNT-GO provided a significant increase in the peak current for ATOR oxidation, proving that VACNT-GO is a useful electrode material.

3.3. Effect of the supporting electrolyte and pH

Cyclic voltammetric studies were carried out in order to identify the optimal supporting electrolyte composition for the electrochemical determination of ATOR using the VACNT-GO electrode. For this, different electrolytes were tested using a fixed 5.0×10^{-5} mol L^{-1} ATOR concentration. The electrolytes were: (i) 0.1 mol L^{-1} KCl, (ii) 0.2 mol L^{-1} acetate buffer (pH_{cond} 4.5), (iii) 0.04 mol L^{-1} Britton–Robinson (BR) buffer (pH_{cond} 4.5), (iv) 0.2 mol L^{-1} phosphate buffer (pH_{cond} 4.5), (v) H_2SO_4 0.1 mol L^{-1} and (vi) 0.5 mol L^{-1} H_2SO_4. From the potential and current peak values obtained for ATOR oxidation, it was concluded that the phosphate buffer solution produced the highest peak current; however the ATOR oxidation potential was slightly shifted to more positive values compared to the other electrolytes (Fig. S4, ESI†). Taking into account the analytical purpose of this work, we chose to work with phosphate buffer solution as the supporting electrolyte.

Next, the effect of the pH_{cond} of the 0.2 mol L^{-1} phosphate buffer was studied in the range 2.0–8.0. The cyclic voltammograms obtained for each pH (Fig. S5, ESI†) demonstrated that the pH directly influenced the ATOR oxidation reaction. The ATOR oxidation peak current seen previously produced an even higher analytical signal in acidic solutions, and with the increase of pH this signal gradually decreased, until at pH 8.0 no more signal was obtained. Thus, 0.2 mol L^{-1} buffer

Table 1 Comparison between the analytical parameters obtained for the proposed voltammetric procedure and other electroanalytical procedures reported in the literature for ATOR[a]

Electrode	Technique	Linear range (nmol L^{-1})	LOD (nmol L^{-1})	Ref.
GCE	DPV	9.65×10^2 to 3.86×10^4	211.0	35
GCE	SWV	9.65×10^2 to 3.86×10^4	205.0	35
BDD	DPV	9.65×10^2 to 3.86×10^4	227.0	35
BDD	SWV	9.65×10^2 to 3.86×10^4	131.0	35
GCE	DPV	2.00×10^3 to 1.00×10^5	595.0	36
GCE	SWV	2.00×10^3 to 1.00×10^5	470.0	36
CPE-CTAB	DPV	5.0×10^1 to 1.00×10^4	4.08	
VACNT-GO	DPAdSV	9.0×10^1 to 3.81×10^3	9.40	This work

[a] GCE – glassy carbon electrode; DPV – differential pulse voltammetry; SWV – square wave voltammetry; BDD – boron-doped diamond; CPE – carbon paste electrode; CTAB – cetyltrimethyl ammonium bromide.

Table 2 Effect of possible interferents on the voltammetric determination of 5.0×10^{-7} mol L^{-1} ATOR solution

Excipient	Proportion (ATOR–excipient)	RSD (%)
Microcrystalline cellulose	1 : 1	+2.0
	1 : 10	−5.1
Sodium croscarmelose	1 : 1	+0.9
	1 : 10	+2.3
Monohydrated lactose	1 : 1	+0.2
	1 : 10	+3.3
Magnesium stearate	1 : 1	−0.2
	1 : 10	+0.9
Calcium carbonate	1 : 1	−1.8
	1 : 10	−8.6

Table 3 Results obtained for the addition/recovery tests of ATOR in pharmaceutical samples[a]

	ATOR ($\times 10^{-6}$ mol L^{-1})		
Sample	Added	Measured	Recovery (%)
I	1.00	1.06 ± 0.08	106
	2.00	1.87 ± 0.09	93.4
II	1.00	1.04 ± 0.07	104
	2.00	1.83 ± 0.08	91.5
III	1.00	1.2 ± 0.1	116
	2.00	2.0 ± 0.1	100

[a] Each addition was repeated and measured independently 3 times to obtain an average value and its associated uncertainty (standard deviation).

phosphate (pH_{cond} 2.0) was chosen as the supporting electrolyte for further experiments.

The inset of Fig. S5 (ESI†) is a plot of oxidation potential (E_p) *versus* pH in the range 2.0–7.0. A linear relation between E_p and pH was obtained in the pH interval from 2.0 to 7.0, following eqn (1):

$$E_p = 1.16 - 0.032\ pH \quad (1)$$

The slope (0.032 V per pH) from eqn (1) was close to the theoretical value, 0.0296 V per pH, indicating that two electrons and one proton are involved in the rate-determining step.[35–37] This observation provides evidence supporting the electro-oxidation reaction that was proposed for ATOR (Fig. 3) involving the oxidation of the pyrrole ring.[21]

3.4. Effect of the pre-concentration potential and time

The effect of the pre-concentration potential and time on the voltammetric response for a 5.0×10^{-5} mol L^{-1} ATOR solution on the VACNT-GO electrode was also investigated. The effect of these were studied using potentials in the range from 0.0 V to + 0.8 V, while maintaining the pre-concentration time at 60 s. The peak currents for ATOR oxidation produced in this range of pre-concentration potentials were nearly constant (Fig. S6(a), ESI†). Thus, in subsequent pre-concentration steps, no potential was applied, and the 'open-circuit potential' was adopted as the standard procedure. The pre-concentration time was then evaluated in the range from 30 to 300 s. The peak current increased until 180 s (Fig. S6(b), ESI†), then remained nearly constant for higher pre-concentration times, indicating a saturation of the electrode surface by the analyte molecules. Therefore, a pre-concentration time of 180 s was selected for further studies.

3.5. Determination of kinetic parameters for ATOR oxidation: α and k_s

In order to determine the kinetic parameters of the electron-transfer process for the ATOR oxidation on the VACNT-GO electrode, cyclic voltammetric experiments were performed at different scan rates. The Laviron's theory for irreversible processes[49] was then applied to calculate the charge-transfer coefficient (α) and the heterogeneous electron-transfer rate constant (k_s). The voltammograms recorded at different scan rates are presented in Fig. 4. According to the Laviron's approach, for irreversible systems the peak potential, E_p, is linearly dependent on the logarithm of the scan rate, v (eqn (2)):[49]

$$E_p = E^0 - \left(\frac{RT}{\alpha nF}\right)\ln\left(\frac{RTk_s}{\alpha nF}\right) + \left(\frac{RT}{\alpha nF}\right)\ln v \quad (2)$$

Table 4 Determination of ATOR in 3 commercial pharmaceutical samples (I, II and III) by the voltammetric (*V*) and comparative (*C*) methods[a]

	ATOR (mg per tablet)				
Sample	Labelled value, *L*	Comparative method, *C*	Voltammetric method, *V*	RSD_1 (%)	RSD_2 (%)
I	10.0	10.9 ± 0.2	10.5 ± 0.7	−3.7	+5.0
II	20.0	21.1 ± 0.9	21.4 ± 0.8	+1.4	+7.0
III	20.0	19.3 ± 0.4	19.6 ± 0.3	+1.6	−2.0

[a] The 'Labelled value' (*L*) is the ATOR concentration (in mg per tablet) quoted by the manufacturers of each sample. Each measurement was repeated independently 3 times to obtain an average value and its associated uncertainty (standard deviation). RSD_1 is a relative standard deviation comparison between the measurements made by the two methods: $RSD_1 = 100 \times (V - C)/C$. RSD_2 is a relative standard deviation comparison between the measurements made by the voltammetric method and the labelled value: $RSD_2 = 100 \times (V - L)/L$.

where α is the charge-transfer coefficient, k_s is the heterogeneous electron-transfer rate constant, F is the Faraday constant, R the gas constant, n is the number of electrons transferred, and E^0 is the standard potential. A linear relationship (correlation, $r = 0.998$) between E_p and ln v was obtained in the range from 10 to 200 mV s^{-1} as shown in the inset of Fig. 4, according to the following linear equation (eqn (3)):

$$E_p = 1.19 + 0.026 \ln v \quad (3)$$

Comparing the slope obtained from eqn (3) with the slope of the Laviron's equation (eqn (2)), with $T = 298.15$ K, αn was calculated to be 0.99. By studying the variation of the peak potential for ATOR oxidation as a function of pH we determined that two electrons are involved in the ATOR oxidation. Therefore, $\alpha \approx 0.5$.

Next, k_s was calculated by comparing the linear coefficient in eqn (3) with the linear coefficient given by Laviron's equation (eqn (2)). The value of $E^0 = 1.058$ V was obtained from the intercept of a plot of E_p *versus* v. From this, k_s was calculated to be 0.26 s^{-1}. This indicates the efficiency of the VACNT-GO electrode in promoting the electron transfer between ATOR and the electrode surface.

3.6. Determination of ATOR by differential pulse adsorptive stripping voltammetry

The voltammetric method for ATOR sensing using the VACNT-GO electrode was applied in the DPAdSV technique. All the experimental parameters influencing this technique were optimised in 0.2 mol L^{-1} buffer phosphate (pH_{cond} 2.0) solution in the presence of 5.0×10^{-5} mol L^{-1} ATOR using a pre-concentration time of 180 s, these being: scan rate potential (2.5 mV $s^{-1} \leq v \leq 20.0$ mV s^{-1}), pulse amplitude (10 mV $\leq a \leq$ 100 mV) and modulation time (5 ms $\leq t \leq$ 20 ms). The optimal value of each parameter was selected taking into account the highest intensity of the anodic peak current and a better signal resolution with a lower contribution from the background current. Thus, the selected values for each parameter were: $v = 10$ mV s^{-1}, $a =$ 90 mV and $t = 10$ ms.

Fig. 5 presents the DPAdS voltammograms measured for different ATOR concentrations as well as the analytical curve obtained (Fig. 5 – inset). The current increases linearly with the concentration of ATOR from 90 to 3.81×10^3 nmol L^{-1} following the linear regression equation ΔI_p (μA) = 8.1 + 1.8 × 10^{-2} [ATOR] (nmol L^{-1}) (with a correlation of $r = 0.996$), with a limit of detection (LOD) of 9.4 nmol L^{-1}. The LOD was calculated using the relation $3 \times \sigma/m$, where σ is the standard deviation of ten blank (electrolyte only) measurements and m is the slope of the analytical curve.

Other electroanalytical procedures have been proposed for the analysis of ATOR, using different materials for the electrodes, and each of these variations has a different LOD and linear response range. The analytical parameters obtained in these procedures were compared with the new DPAdSV method (Table 1). As can be seen, the procedure using the VACNT-GO electrode and DPAdSV technique provided a linear analytical range comparable to those obtained using glassy carbon and boron-doped diamond electrodes, and a LOD lower than all obtained with these electrodes.[35,36] Abbar and Nandibewoor[37] using a carbon paste electrode reached a greater ATOR concentration range and a LOD slightly lower than that

Table 5 Results obtained for voltammetric determination of ATOR in synthetic urine and human serum samples[a]

	ATOR ($\times 10^{-7}$ mol L^{-1})		
Sample	Known amount added	Amount measured	Recovery (%)
Urine	7.0	7.8 ± 0.1	111
	20.0	19.0 ± 1	95.0
Human serum	7.0	7.2 ± 0.5	103
	20.0	19.2 ± 0.3	96.0

[a] Each measurement was repeated independently 3 times to obtain an average value and its associated uncertainty (standard deviation).

achieved in this work. However, an activation pre-step for the electrode was necessary and the surfactant cetyltrimethyl ammonium bromide had to be used as an enhancing agent. This is a more complex procedure compared to the method proposed in this work, which has a LOD of the same magnitude without the use of a compound of this class. Furthermore, it is emphasized that the analytical parameters obtained in this work are sufficient to quantify ATOR in commercial pharmaceutical and biological samples, as will be presented in the next section.

The intra-day and inter-day repeatability of the voltammetric procedure were investigated. For intra-day repeatability, 10 successive measurements were performed for two solutions of different ATOR concentrations (6.0×10^{-7} mol L^{-1} and 1.5×10^{-6} mol L^{-1}), giving relative standard deviations (RSD) of 2.3% and 2.2% for peak current measurements. The inter-day repeatability was also studied using two ATOR concentrations (6.0×10^{-7} mol L^{-1} and 1.5×10^{-6} mol L^{-1}) but several measurements were made over 3 days, yielding RSD values of 6.0% and 5.9%. Thus, the proposed analytical method using a VACNT-GO electrode and the DPAdSV technique was demonstrated to exhibit good precision. Moreover, the repeatability of the manufacturing of two different VACNT-GO electrodes in the presence of 6.0×10^{-7} mol L^{-1} and 1.5×10^{-6} mol L^{-1} ATOR solutions in 0.2 mol L^{-1} buffer phosphate (pH_{cond} 2.0) was also the object of study of this work. The RSD were 9.9% and 11.5% respectively, indicating a good repeatability of the preparation of the proposed sensor.

3.7. Studies of excipients and addition/recovery tests

The potential interference of some excipient compounds typically found in ATOR pharmaceutical formulations was studied for the following excipients: microcrystalline cellulose, croscarmellose sodium, lactose monohydrate, magnesium stearate and calcium carbonate. To evaluate the effect of these compounds on the voltammetric response, analysis was carried out of a 5.0×10^{-7} mol L^{-1} ATOR solution in the presence of these excipients at two different proportions, 1 : 1 and 1 : 10 (analyte–excipient). Table 2 shows the RSD obtained in the presence of each excipient, where the RSD values were calculated by comparing the analytical signals obtained from the ATOR solution in the presence and absence of each excipient. The excipients did not influence the voltammetric ATOR determination. These results were confirmed by the addition and recovery studies presented below.

In order to investigate the effect of the matrix materials used in commercial pharmaceutical samples on the voltammetric response, studies were performed by addition and recovery tests. Three ATOR pharmaceutical samples were used, and the addition/recovery tests were carried out using two ATOR concentrations: 1.0×10^{-6} mol L^{-1} and 2.0×10^{-6} mol L^{-1}. From Table 3 it can be seen that recoveries ranging from 91.5 to 116% were obtained, demonstrating that the proposed procedure does not suffer significant interference from the sample matrix, and that it is therefore selective for ATOR determination.

3.8. Determination of ATOR in pharmaceutical and biological samples

The voltammetric method developed using a VACNT-GO electrode and DPAdSV was applied in the determination of ATOR in commercial pharmaceutical samples. The samples were also analysed by the spectrophotometric comparative method, and the results for both methods are given in Table 4. The results obtained for the two methods were compared by applying the paired *t*-test, at a confidence level of 95%. The $t_{experimental}$ value (0.257) was lower than the $t_{critical}$ value (2.776), and therefore it can be concluded that there is no statistically significant difference between the results obtained using the two analytical methods. Moreover, the RSD between the methods (RSD_1) ranged from −3.7% to +1.6%, and between the values determined by the proposed method and the labelled values (RSD_2) ranged from −2.0% to +7.0%. These results demonstrate the excellent accuracy of the voltammetric procedure and its effectiveness in the quantification of ATOR in commercial pharmaceutical samples.

In addition, the voltammetric method was also used for ATOR determination in two synthetic biological samples, urine and human serum. Two ATOR concentrations, 7.0×10^{-7} mol L^{-1} and 2.0×10^{-6} mol L^{-1}, were added to these samples, and the results of their analyses are given in Table 5. For these samples very satisfactory recoveries were obtained from 96.0% to 111%, which suggests the potential of the proposed procedure for ATOR determination in biological samples.

4. Conclusions

We have described a novel method for the production of highly porous vertically aligned CNT, which have had their tips exfoliated by oxygen plasma etching. The O_2 plasma also attaches oxygen groups onto the tips and changes the hydrophilicity of the material in a manner which is very attractive for electrochemical applications. We studied the electrode behaviour of this material for ATOR determination by DPAdSV. Excellent accuracy for the detection of low concentrations of ATOR, with an LOD of 9.4 nmol L^{-1} was achieved with the porous and superhydrophilic VACNT-GO electrodes. This value was obtained by linear regression in the concentration range from 90 to 3.81×10^3 nmol L^{-1} using optimized parameters, such as open-circuit potential with pre-concentration time of 180 s at pH_{cond} 2.0. Laviron's theory for irreversible processes was employed to calculate the kinetic parameters for the electro-oxidation of ATOR on the VACNT-GO electrode. The charge transfer coefficient $\alpha \approx 0.5$ and the heterogeneous electron transfer rate $k_s = 0.26\ s^{-1}$ were calculated. A mechanism for the electro-oxidation of ATOR is proposed involving two electrons and one proton in the rate-determining step. Although preliminary, these experiments have shown that such VACNT-GO may be excellent candidates for electrode materials, and can be used to determine the concentration of ATOR in both commercial pharmaceutical samples and biological samples such as urine and plasma. There are still a number of parameters that need to be investigated to improve and optimize the

electrochemical performance of these electrodes, such as the length and packing density of the CNT, the substrate composition, residence time of the electrode and the reactor pressure during oxygen plasma etching, *etc.* And the utility of these electrodes is not limited to ATOR – we are currently investigating their use for the analysis of a variety of other biologically and environmentally important molecules.

Acknowledgements

We gratefully acknowledge the LME/LNLS-Campinas for microscopy support and mainly to Brazilian agencies CNPq (202439/2012-7) for financial support. A major thanks to Prof. Paul W. May of the School of Chemistry (University of Bristol) for the improvement of the written work.

References

1 M. Paradise and T. Goswami, *Mater. Des.*, 2007, **28**, 1477–1489.
2 J. Wang, *Electroanalysis*, 2005, **17**, 7–14.
3 N. Punbusayakul, *Procedia Eng.*, 2012, **32**, 683–689.
4 F. C. Vicentini, B. C. Janegitz, C. M. A. Brett and O. Fatibello-Filho, *Sens. Actuators, B*, 2013, **188**, 1101–1108.
5 B. C. Janegitz, R. Pauliukaite, M. E. Ghica, C. M. A. Brett and O. Fatibello-Filho, *Sens. Actuators, B*, 2011, **158**, 411–417.
6 I. Taurino, S. Carrara, M. Giorcelli, A. Tagliaferro and G. De Micheli, *Sens. Actuators, B*, 2011, **160**, 327–333.
7 A. Chou, T. Bocking, N. K. Singh and J. J. Gooding, *Chem. Commun.*, 2005, 842–844.
8 P. Yáñez-Sedeño, J. M. Pingarrón, J. Riu and F. X. Rius, *TrAC, Trends Anal. Chem.*, 2010, **29**, 939–953.
9 C. E. Banks, T. J. Davies, G. G. Wildgoose and R. G. Compton, *Chem. Commun.*, 2005, 829–841.
10 I. Dumitrescu, P. R. Unwin and J. V. Macpherson, *Chem. Commun.*, 2009, 6886–6901.
11 Y. Liu, Z. Wu, X. Chen, Z. Shao, H. Wang and D. Zhao, *J. Mater. Chem.*, 2012, **22**, 11908–11911.
12 J. J. Gooding, A. Chou, J. Liu, D. Losic, J. G. Shapter and D. B. Hibbert, *Electrochem. Commun.*, 2007, **9**, 1677–1683.
13 F. C. Moraes, T. A. Silva, I. Cesarino and S. A. S. Machado, *Sens. Actuators, B*, 2013, **177**, 14–18.
14 N. Jia, Z. Wang, G. Yang, H. Shen and L. Zhu, *Electrochem. Commun.*, 2007, **9**, 233–238.
15 S. Shanmugam and A. Gedanken, *J. Phys. Chem. B*, 2006, **110**, 2037–2044.
16 P. J. Britto, K. S. V. Santhanam, A. Rubio, J. A. Alonso and P. M. Ajayan, *Adv. Mater.*, 1999, **11**, 154–157.
17 K. Yu, G. Lu, Z. Bo, S. Mao and J. Chen, *J. Phys. Chem. Lett.*, 2011, **2**, 1556–1562.
18 T. A. Silva, H. Zanin, E. Saito, R. A. Medeiros, F. C. Vicentini, E. J. Corat and O. Fatibello-Filho, *Electrochim. Acta*, 2014, **119**, 114–119.
19 E. Saito, E. F. Antunes, H. Zanin, F. R. Marciano, A. O. Lobo, V. J. Trava-Airoldi and E. J. Corat, *J. Electrochim. Soc*, 2014, **161**, H321–H325.
20 J.-S. Ye, Y. Wen, W. De Zhang, L. M. Gan, G. Q. Xu and F.-S. Sheu, *Electroanalysis*, 2003, **15**, 1693–1698.
21 J.-S. Ye, Y. Wen, W. De Zhang, L. Ming Gan, G. Q. Xu and F.-S. Sheu, *Electrochem. Commun.*, 2004, **6**, 66–70.
22 B. Xu, M.-L. Ye, Y.-X. Yu and W.-D. Zhang, *Anal. Chim. Acta*, 2010, **674**, 20–26.
23 Y. Wang, G. Du, L. Zhu, H. Liu, C.-P. Wong and J. Wang, *Sens. Actuators, B*, 2012, **174**, 570–576.
24 Y.-M. Liu, H.-H. Pu, G.-Y. Liu, J.-Y. Jia, L.-P. Weng, R.-J. Xu, G.-X. Li, W. Wang, M.-Q. Zhang, C. Lu and C. Yu, *Clin. Ther.*, 2010, **32**, 1396–1407.
25 A. Moscardó, J. Vallés, A. Latorre, I. Madrid and M. T. Santos, *Thromb. Res.*, 2013, **131**, e154–e159.
26 S. Ertürk, A. Önal and S. Müge Çetin, *J. Chromatogr. B: Anal. Technol. Biomed. Life Sci.*, 2003, **793**, 193–205.
27 L. Nováková, D. Šatínský and P. Solich, *TrAC, Trends Anal. Chem.*, 2008, **27**, 352–367.
28 E. Guihen, G. D. Sisk, N. M. Scully and J. D. Glennon, *Electrophoresis*, 2006, **27**, 2338–2347.
29 M. M. AlShehri, *Saudi Pharm. J.*, 2012, **20**, 143–148.
30 M. M. K. Sharaf El-Din, F. M. M. Salama, M. W. I. Nassar, K. A. M. Attia and M. M. Y. Kaddah, *J. Pharm. Anal.*, 2012, **2**, 200–205.
31 H. W. Darwish, S. A. Hassan, M. Y. Salem and B. A. El-Zeiny, *Spectrochim. Acta, Part A*, 2011, **83**, 140–148.
32 S. Mazurek and R. Szostak, *J. Pharm. Biomed. Anal.*, 2009, **49**, 168–172.
33 E. T. G. Cavalheiro, C. M. A. Brett, A. M. Oliveira-Brett and O. Fatibello-Filho, *Bioanal. Rev.*, 2012, **4**, 31–52.
34 G. G. Oliveira, D. C. Azzi, F. C. Vicentini, E. R. Sartori and O. Fatibello-Filho, *J. Electroanal. Chem.*, 2013, **708**, 73–79.
35 B. Dogan-Topal, B. Uslu and S. A. Ozkan, *Comb. Chem. High Throughput Screening*, 2007, **10**, 571–582.
36 B. Dogan-Topal, B. Bozal, B. T. Demircigil, B. Uslu and S. A. Ozkan, *Electroanalysis*, 2009, **21**, 2427–2439.
37 J. C. Abbar and S. T. Nandibewoor, *Colloids Surf., B*, 2013, **106**, 158–164.
38 H. Zanin, P. May, D. J. Fermin, D. Plana, S. M. C. Vieira, W. I. Milne and E. J. Corat, *ACS Appl. Mater. Interfaces*, 2014, **6**, 990–995.
39 A. O. Lobo, H. Zanin, I. A. W. B. Siqueira, N. C. S. Leite, F. R. Marciano and E. J. Corat, *Mater. Sci. Eng., C*, 2013, **33**, 4305.
40 A. Mateti, M. K. Thimmaraju and N. Raghunandan, *International Journal of Institutional Pharmacy and Life Sciences*, 2012, **2**, 255–264.
41 N. Laube, B. Mohr and A. Hesse, *J. Cryst. Growth*, 2001, **233**, 367–374.
42 H. Parham and B. Zargar, *Talanta*, 2001, **55**, 255–262.
43 H. Zanin, P. W. May, A. O. Lobo, E. Saito, J. P. B. Machado, G. Martins, V. J. Trava-Airoldi and E. J. Corat, *J. Electrochem. Soc.*, 2014, **161**, H290–H295.
44 E. F. Antunes, A. O. Lobo, E. J. Corat, V. J. Trava-Airoldi, A. A. Martin and C. Veríssimo, *Carbon*, 2006, **44**, 2202–2211.
45 E. F. Antunes, A. O. Lobo, E. J. Corat and V. J. Trava-Airoldi, *Carbon*, 2007, **45**, 913–921.

46 S. Kundu, Y. Wang, W. Xia and M. Muhler, *J. Phys. Chem. C*, 2008, **112**, 16869–16878.
47 O. C. Compton and S. T. Nguyen, *Small*, 2010, **6**, 711–723.
48 H. Zanin, E. Saito, H. J. Ceragioli, V. Baranauskas and E. J. Corat, *Mater. Res. Bull.*, 2014, **49**, 487–493.
49 E. Laviron, *J. Electroanal. Chem. Interfacial Electrochem.*, 1979, **101**, 19–28.